# Lattice density functional theory investigation of pore shape effects. II. Adsorption in collections of noninterconnected pores

A. P. Malanoski and Frank van Swol
*Department of Chemical and Nuclear Engineering, University of New Mexico, Albuquerque, New Mexico 87106*
*and Sandia National Laboratories, Albuquerque, New Mexico 87185*
(Received 13 June 2002; published 10 October 2002)

A fully explicit three-dimensional lattice density functional theory is used to investigate adsorption behavior in collections of noninterconnected pores. The study focuses on the effects of external surfaces and the shape of individual pores on the adsorption and desorption isotherms. Pore shapes far more varied than the traditionally considered cylinders and slitlike pores allow a better assessment of the general role of pore geometry. Pore shapes that exhibit acute angles display significantly different adsorption and desorption branches. For most pores the presence of an exterior surface greatly reduces the extent of the hysteresis loop through meniscus formation. However, for sufficiently large pores a thick film present on the exterior surface can interfere with meniscus formation and lead to desorption controlled by the thick film. A comparison was made with recent experiments on well-characterized systems of noninterconnected pores. The calculations do not agree with the experimental adsorptions if the models are based on the pore types suggested by the experimental work. Improved agreement can be obtained by considering small bottlenecks along the length of the pores length. To establish the presence of such a feature would probably require more detailed experimental characterization.

DOI: 10.1103/PhysRevE.66.041603 PACS number(s): 68.43.−h, 64.70.Fx, 02.50.Ng

## I. INTRODUCTION

This paper completes a study begun in our first paper, hereafter referred to as Part I, of the adsorption behavior of pore shapes different from those that are usually studied, i.e., slit or cylindrical [1]. Part I investigated the behavior of individual pores as the size and shape was varied. This work was motivated by recent experimental work, as discussed in Part I [2–4], and by the fact that independent pore models of the cylinders produce an adsorption isotherm which does not agree with the experimental data. In this work we study pore distributions of various pore shapes which were described as individual pores in Part I and which are in the size range relevant to the experimental measurements. In particular, we investigate whether departures from ideal geometries can explain the experimental data.

## II. MODEL AND METHOD OF SOLUTION

A three-dimensional single occupancy lattice density functional model was used to investigate adsorption behavior in various pore shapes. The model allows for a mean field square-well-type attraction for neighboring sites on a lattice. For this study a simple cubic lattice was used. The details of the model are reported in Part I. For reasons of computational efficiency, we chose to use a model where the fluid-fluid interaction was present only for the nearest neighboring lattice sites. The simulations were run at a $T/T_c$ of 0.583 which is similar to the value of the experimental work (0.609). The strength of the wall-fluid interaction was then tuned so that the adsorption behavior at low pressures was qualitatively similar to the experimental behavior. We expect only limited quantitative agreement at this time since we are using only a nearest neighbor interaction and a coarse lattice. The wall-fluid interaction was a Lennard-Jones 12-6 potential rather than a square well as these interactions were only evaluated once per isotherm; we used a cutoff of $6\sigma$ for this potential, where $\sigma$ is the lattice site separation. Because this is a single occupancy model, all fluids are approximated by spherical molecules which in the case of nitrogen means $\sigma \approx 0.4$–$0.5$ nm. We determined the wall-fluid interaction for this system at the point where complete wetting occurs on a planar wall and found it to be $\epsilon_w/\epsilon_f = 0.38$. The value required to qualitatively reproduce the adsorption behavior at low pressures was $\epsilon_w/\epsilon_f = 1.31$. We chose to study square, cylindrical, triangular, and rectangular pores, some of which can only be approximated on a simple cubic lattice. For the case of the square pores, the walls could be smooth or surface roughness could be introduced by having 50% of the next surface layer randomly filled with wall sites. We made cylindrical pores on the simple cubic lattice by choosing a center point and removing all complete lattice sites that were located inside a specified radius. 90° isosceles triangular pores were made by filling in half of a square pore along the diagonal.

## III. RESULTS

Because the theory we are using is fully explicit for three dimensions and can be solved relatively quickly, it is feasible to directly model a collection of pores. Figure 1 has isocurvature plots of densities greater than 0.2 for two different conditions, as viewed straight down the axis of a collection of square and cylindrical pores. For the moment, consider Fig. 1(b) which is at a higher temperature and a stronger wall-fluid interaction. The smallest pores have capillary condensed and the intermediate sized pores have formed thicker layers than the largest pores. A film forms on the exterior surface but gets thinner near pore openings, as indicated by the variation in the gray-scale color around each pore. Some

 

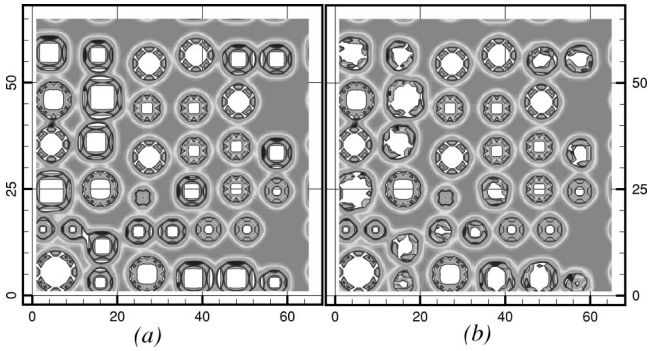


FIG. 1. Pictures $a(T=0.875)$ and $b(T=1.23)$ are three-dimensional (3D) isodensity curvature plots, with contours drawn for densities greater than 0.2, for a collection square and cylindrical pores. The view is straight down the pore axis. The dimensions are in units of $\sigma$.

of the pores that are closer together have a joint band around them. The walls separating the pores were at least three lattice sites thick, so the fluid which is restricted to a much shorter length interaction cannot interact through the pore walls. The wall interaction has a cutoff of $6\sigma$ and some of the walls around pores are not this thick, which causes a nonuniform film thickness in the pores which can be seen on close examination. At the lower temperature and wall strength shown in picture Fig. 1, these nonuniformities in the film thickness are not as apparent as at the higher temperature and wall strength. This is due to the fact that at the lower temperature and wall strength the attractive contribution from wall sites further from the surface is smaller, and since all the surfaces have no missing wall sites closer in, the variation in film thickness is reduced. In Fig. 2, isocurvature plots at a saturation lower than and higher than the saturation of Fig. 1 are shown at the lower temperature of 0.875. Figure 1(a) can be slightly confusing at first as only the fluid at densities greater than 0.2 are shown, and at this saturation some sections of the exterior surface do not reach this density. It is then difficult to distinguish the pores from these empty surface regions, although comparisons with the other images resolve this confusion. The largest sections of the

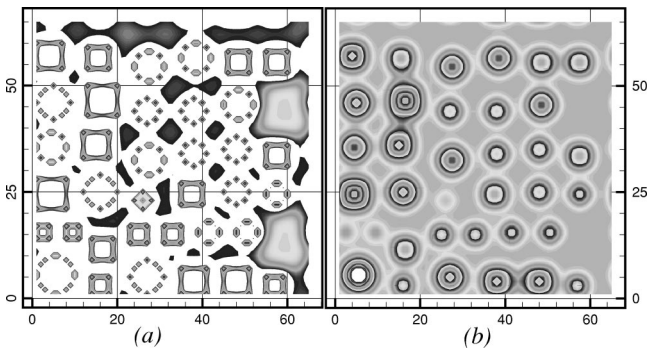


FIG. 2. Pictures *a* and *b* are 3D isodensity curvature plots, with contours drawn for densities greater than 0.2, for a collection square and cylindrical pores at a temperature of 0.875. The view is straight down the pore axis. *a* is at a lower saturation that of Fig. 1(b) and *d* is at a higher saturation. The dimensions are in units of $\sigma$.

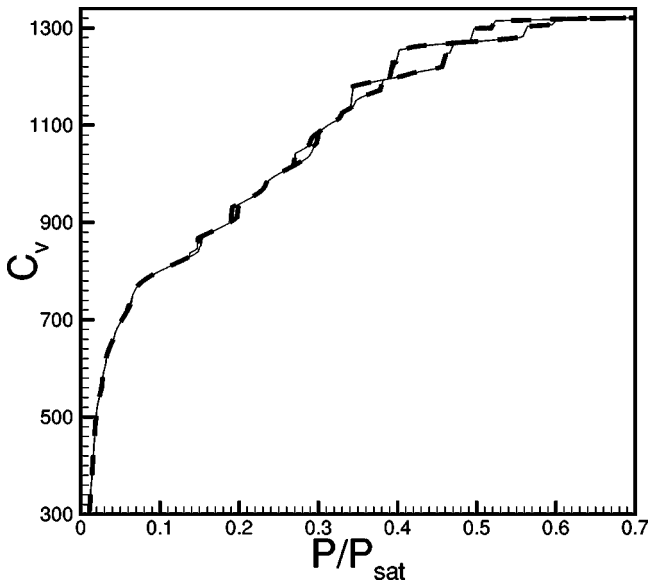


FIG. 3. Adsorption in the center slice $C_v$ versus saturation $P/P_{sat}$ for the explicit collection of pores (solid line) and the adsorption computed from individual pores (thick dashed line) $[C_v \equiv (\sigma/z_l)\int_{z'}^{z'+z_l}\int_a \rho(\vec{s},z)d\vec{s}dz$, see text].

surface reach higher densities than some of the smaller sections, hence the variation. Many of the pores do not form complete films but rather only reach a density greater than 0.2 at their most energetic sites (i.e., corners). Figure 2(b) is at a higher saturation than Fig. 1(a) and has more pores that have capillary condensed. The menisci that form are right above the pores and because they are smaller do not form bands around groups of pores. In Fig. 2(b), all of the pores except the largest one have capillary condensed.

The adsorption-desorption curves for this distribution can also be calculated from the single pore results or from the actual collection of pores shown in Figs. 1 and 2. There are advantages and disadvantages to using each method to compute the total adsorption of a group of pores. The collection of pores simulated as a unit allows one to probe the possibility of pores influencing the adsorption in each other. However, to have the correct ratio of various pore sizes present in a collection of pores might require a very large number of pores, which would require a lengthy simulation. Also, the results for one collection of pores are not easily applied to other cases. Single pores have an advantage in this respect in that once the results are calculated they can be used for many different collections of pores. The weakness of the single pore approach is that it is only useful for modeling pores that do not interact with each other. When this is true, it is always advantageous to use single pore results because of their flexibility. The adsorbed material measured in each pore is $C_v \equiv (\sigma/z_l)\int_{z'}^{z'+z_l}\int_a \rho(\vec{s},z)d\vec{s}dz$ where the area $a$ is the cross section of the pore and $z'$ is halfway down the pore length. $\vec{s}$ is a $2d$ vector. $z_l$ is one layer thick for pores without roughness and five layers for rough pores. In Fig. 3 $C_v$ versus the saturation $P/P_{sat}$ is plotted for a collection of pores simulated together and for a distribution of single pores. The results calculated from both methods are indistinguishable.

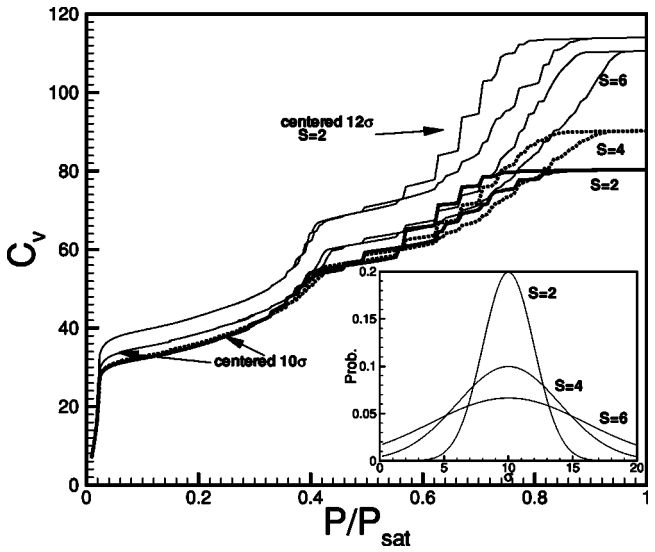


FIG. 4. Adsorption in the center slice $C_v$ (see Fig. 3 caption) versus saturation $P/P_{sat}$ for Gaussian distributions of square pores centered at $10\sigma$ and having standard deviations of 2, 4, and 6. Inset: the figure shows the Gaussian distributions with those standard deviations.

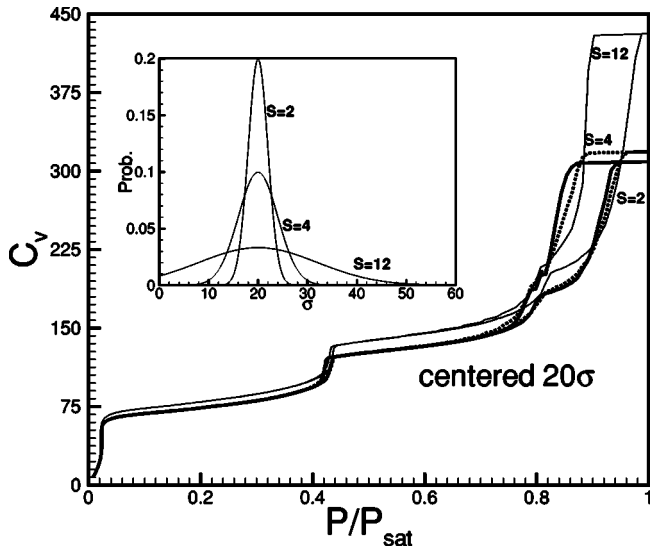


FIG. 5. Adsorption in the center slice $C_v$ (see Fig. 3 caption) versus saturation $P/P_{sat}$ for Gaussian distributions of square pores centered at $20\sigma$ and having standard deviations of 2, 4, and 12. Inset: the figure shows the Gaussian distributions with those standard deviations.

This demonstrates that in this model the pores separated by a sufficient wall thickness behave as a collection of individual pores. As the experimental system is known to be a set of noninteracting pores [3], we will compute the adsorption isotherms for all later collections of pores from the individual pore results.

In order to compare the calculated results to the adsorption isotherms measured experimentally we will consider collections of individual pores. Let us first consider a few examples of pore distributions to understand the general behavior of these pores. For these examples, pore distributions were generated for ideal cylindrical pores. The weighting probability for a given pore in one of the example distributions was the same as that of the cylindrical pore with the same area. In Fig. 4 distributions of square pores were calculated for Gaussian distributions of cylindrical pores centered around $10\sigma$ and with standard deviations of $2\sigma$, $4\sigma$, and $6\sigma$. The distribution centered at $12\sigma$ and a standard deviation of $2\sigma$ is also shown. Because we can only create pores of certain sizes on the lattice, the hysteresis loops for these smaller pores exhibits a distinct stepping. The adsorption curve in the hysteresis loop is steeper at the top of the loop and the desorption curve has a slope similar to that of the adsorption branch. At the bottom of the loop a narrowing of the loop is seen. Similar results have been seen before for ideal geometry pores, and it is considered the typical hysteresis loop expected for collections of independent pores. In Fig. 5 pore distributions are shown centered at $20\sigma$. Similar behavior is seen overall although the curves are much steeper at the end of the hysteresis loop at higher values of the saturation. This is expected as these larger pores contain a much larger fraction of the system volume. The curve for the standard deviation of $12\sigma$ does have a desorption curve which is slightly steeper than the adsorption curve. This is because the largest pores empty at the same saturation as their desorption is controlled by the exterior surface (see Part I). This effect is not pronounced as both curves are so steep. In Fig. 6 the distributions for various pore shapes are shown for a Gaussian distribution centered at $20\sigma$ and having a standard deviation of $4\sigma$. The adsorption behavior at low values of the saturation varies greatly with pore shape, but this is to be expected as distributions were chosen to match the capillary condensation loops. The hysteresis loops do show good agreement with each other, except for the triangular pore which shows a larger deviation as its shape is a larger departure from a cylindrical pore.

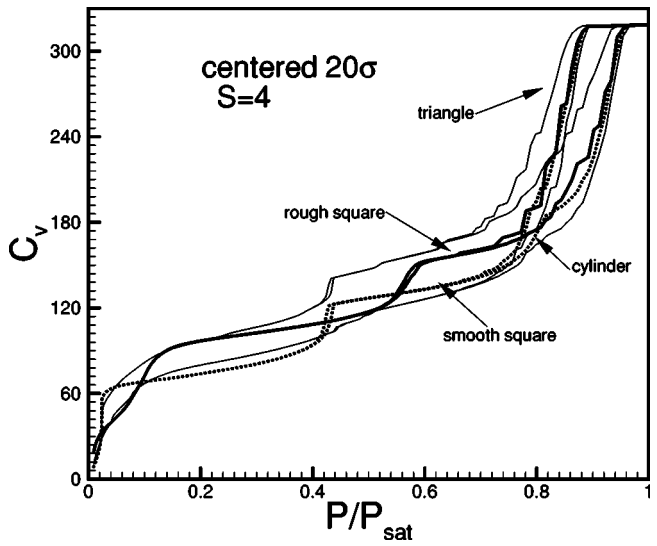


FIG. 6. Adsorption in the center slice $C_v$ (see Fig. 3 caption) versus saturation $P/P_{sat}$ for Gaussian distributions of smooth and rough square pores (thick dotted and solid lines), triangular pores (thin solid line), and cylindrical pores (thin solid line) centered at $20\sigma$ and having a standard deviation of 4.

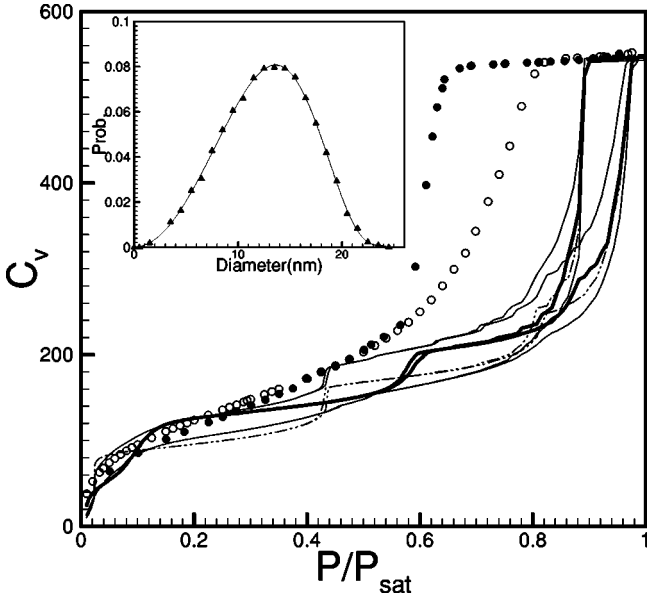


FIG. 7. Adsorption in the center slice $C_v$ (see Fig. 3 caption) versus saturation $P/P_{sat}$ for experimental distributions of smooth and rough square pores (dotted-dashed and thick solid lines), triangular pores (thin solid line), and cylindrical pores (thin solid line). Experimental adsorption (open circles) and desorption (filled circles) results are shown [3]. Inset: shows pore distribution and the polynomial fit.

In the inset of Fig. 7 we show the pore distribution as measured experimentally. Adsorption and desorption curves for the various pore shapes were calculated using this pore distribution. In Fig. 7 we show $C_v$ versus the saturation for distributions of the various pore shapes. The experimental results are also shown. The *y* axis of the experimental results has been rescaled so that both simulation and experimental results give the same value of $C_v$ when all the pores have condensed. The cylindrical, smooth square, and roughened square pores exhibit behavior very similar to each other for the pore filling and emptying. The adsorption branch begins to steepen as the region in the hysteresis loop is entered. At the high saturation end of the hysteresis loop a large distinct jump is seen as the largest pores fill. Pore condensation occurs at a lower saturation for the triangular pore. The distinct jump at the high saturation end of the hysteresis loop is not as large as that seen for the other pore shapes because more filling occurs at lower saturations. The main difference between the triangular pores and other shapes is the presence of acute angle corners which form wedges along the pore length. As the saturation increases, these acute wedges fill in a manner different from the right or obtuse angle wedges found in the other pore shapes.

Let us now assess how well the simulations reproduce the experimental results. At low saturations the shape and behavior of the experimental results is matched well by all the pore shapes except for the smooth square pores. All of the pore shapes have surface variation and/or roughness on a short length scale except for the smooth square pore. This type of variation on a short length scale accounts for the adsorption behavior of the experimental results at low saturations. The most significant feature of all the simulation results is that the location where the pore distributions fill and empty is significantly different from the experimental results. The overall size of the hysteresis loop also differs greatly between the simulation results and the experimental result. The slopes of the adsorption and desorption branches in the simulation results are very similar while they differ greatly in the experimental results. The shape of the adsorption curve of the triangular pores better reproduces the curvature changes seen in the experimental results than any of the other pore shapes. The experimental and simulated desorption branches share a common shape which is very steep. However, not much weight can be placed on this as the steepness of the simulation results is due to the large size of the pores as discussed previously. The cause of the sharp desorption branch and its location for the experimental results cannot be readily explained.

There are several possible remedies that must be considered before concluding that the simulations are not capable of reproducing the experimental results. The main issues are the chosen simulation temperature, the units that the experimental results are published in, the possibility of a stable film on the exterior surface, the shape of the simulation pores, the details of the wall potential, and the details of the fluid-fluid interaction.

*Temperature*. Since the principle of corresponding states is applicable for this system, it is most proper to compare simulation and experimental systems based on $T/T_c$. The simulation results were calculated at a slightly lower $T/T_c$ than the experiments, so the simulation temperature could be increased which may shift the filling of all the pores. The problem that is not addressed by increasing the temperature is that the size of the hysteresis loop decreases as the temperature increases, which would further increase the discrepancy in when the pores empty. In Fig. 8, the adsorption $C_v$ versus the saturation is shown for a square pore at the simulation $T/T_c=0.583$, the experimental $T/T_c=0.609$, and for $T/T_c=0.3333$, 0.5, and 0.9. The result at the same $T/T_c$ as the experiment showed no significant shifts in the location of the pore condensation. This all leads to the conclusion that the simulation temperature is not introducing any significant errors in the results, and this cannot account for the differences between the experimental results and simulations. The discrepancy in the adsorption before the pore condensation is not large and this can be accounted for by the model used. A feature of the triangular pore distribution discussed later is that its adsorption branch agrees better with the experimental results at intermediate saturations than any of the other pore shapes.

*Experimental* $P_{sat}$. The experimental results are reported relative to the saturation pressure or the pressure at equilibrium for the two phases [3]. Since in the paper they do not mention how they determined this value there is a slight chance they made an error in determining it. A possible error is taking the pressure at which the filling of the system occurs as the saturation pressure (which depends on the metastability of the system rather than the pressure at equilibrium). If the simulation pressure at the limit of metastability of a vapor above the surface, which occurs at a saturation of

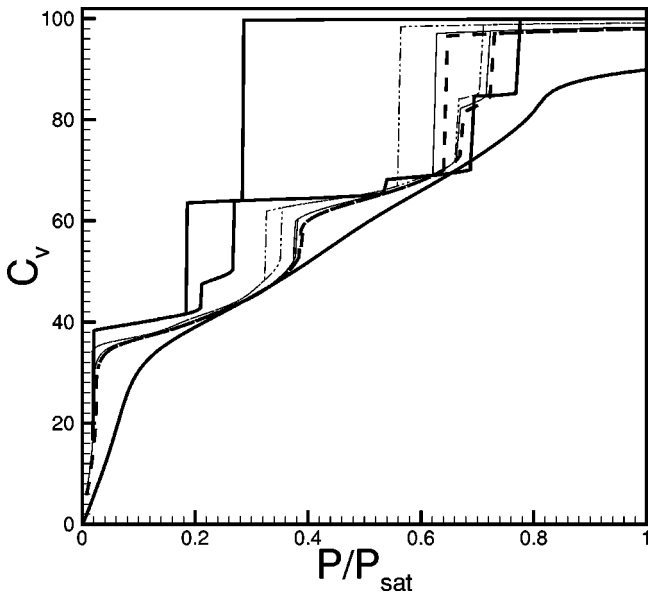


FIG. 8. Adsorption in the center slice $C_v$ (see Fig. 3 caption) versus saturation $P/P_{sat}$ for a smooth square $10\sigma$ pore at a $T/T_c$ of 0.3333 (thick solid line), 0.50 (thin dash-dotted line), 0.583 (thin solid line), 0.609 (thick dashed line), and 0.90 (thick solid line).

1.13, is used as the reference pressure rather than the computed equilibrium saturation pressure, the reported saturations for pore filling and emptying will be shifted to lower saturations. In fact, the pore filling now occurs at roughly the correct saturation. However, the pore emptying is still at too high a saturation compared to the experimental results. While we do not believe it likely that the experimental results have any error in the reported units, it was useful to see if this type of error could account for the discrepancies seen between the simulation and the experimental results.

*Film on exterior surface*. The simulated pores of this work and the experimental pores have pore ends opening onto an exterior surface. It is conceivable that a thick film could form on this exterior surface that would remain metastable as the saturation is lowered. If this film was sufficiently thick, it could prevent the formation of menisci over the pore openings. This would prevent the pores from emptying until the thick film on the exterior surface itself became unstable. If the film was stable to a low enough saturation, such as the saturation reported in the experimental results for the emptying of the pores, it would produce a simulation desorption curve that agrees with the experimental results. This would have no effect on the adsorption behavior of the pores and so could not account for those discrepancies. However, this was considered in Part I, where it was determined that for this model a thick film that would prevent the formation of menisci on the exterior surface only exists until a saturation of 0.9 (i.e., well above where the emptying occurs in the experiment).

*Pore shape*. So far in this paper we have only considered a few shapes beyond that of a cylindrical pore, and none of these shapes exactly match the experimental pore shapes. However, in Part I we did consider several additional shapes and several variations of the shapes. From those results, we

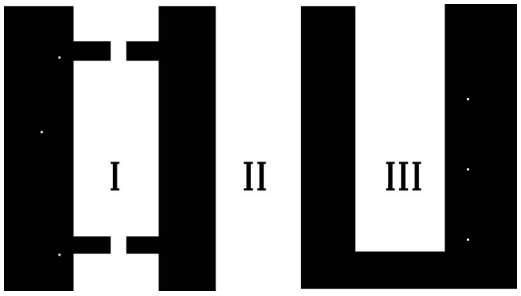


FIG. 9. Schematic of three general pore types. Type I, ink bottle, Type II, straight with both ends open; and Type III, straight with one end open.

are able to conclude that although we had not sampled all possible pore shapes, we had sampled prototypical examples of all the significant ways in which a pore's shape may depart from cylindrical. We have done one arbitrary shaped pore with the results reported in Part I, which has a qualitative behavior very similar to the triangular pores. The other significant variation we investigated was higher aspect ratio rectangular pore shapes. From Part I we know that considering such pores can shift the pore filling to lower saturation. Our conclusion from the simulations done so far and a cursory look at the TEM pictures are that too few of the pores have higher aspect ratios and these aspect ratios are still too small to induce a significant shifting in the saturation at which pore filling occurs. It is possible to match the experimental system more closely but this requires determining the correct distribution of aspect ratio, and pores sizes from a lengthy investigation of the the experimental TEM pictures, followed by simulation of these pore shapes.

*Variations along the pore length*. The question we pose is could simulated pores with variations along their pore length better reproduce the actual experimental results? The results obtained for the triangular pores show that the presence of acute angled corners can account for the overall shape of the adsorption isotherm, even though the shift of the pore condensation to lower saturations and the size of the hysteresis loop and steepness of the desorption branch remain unaccounted for by the simulations. We must consider variations that would not contradict the experimentally gathered information. The experimental work has evidence that supports the conclusion that the pores do not vary in diameter for significant periods down the pore axis, type II in Fig. 9. The evidence for this conclusion was obtained from TEM pictures taken from various points. These always compute the same pore distribution. In addition, the total volume computed from these pore distributions agrees very well with the total adsorption. However, it is conceivable that constrictions exist in the pores that locally reduce the pore diameter but only for an extremely short distance of the total pore length. The chances that such constrictions could be detected in the TEM are negligible and the total volume of the system would be unaffected, so the performed checks are not capable of assessing the presence of such constrictions.

This introduces the possibility of the experimental pores having a different configuration than Type II. The presence of just two such constrictions in every pore close to each

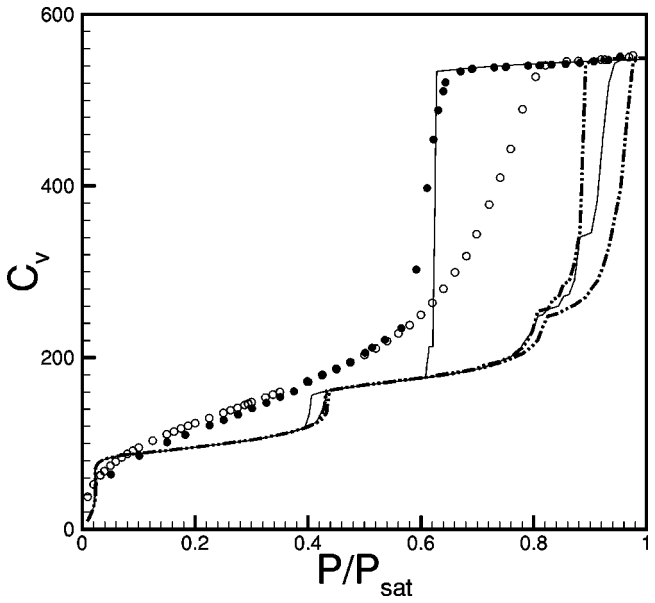


FIG. 10. Adsorption in the center slice $C_v$ (see Fig. 3 caption) versus saturation $P/P_{sat}$ for experimental distributions of smooth square pores (thick dotted-dashed line) and square ink-bottle pores (thin solid line). Experimental adsorption (open circles) and desorption (filled circles) results are shown [3].

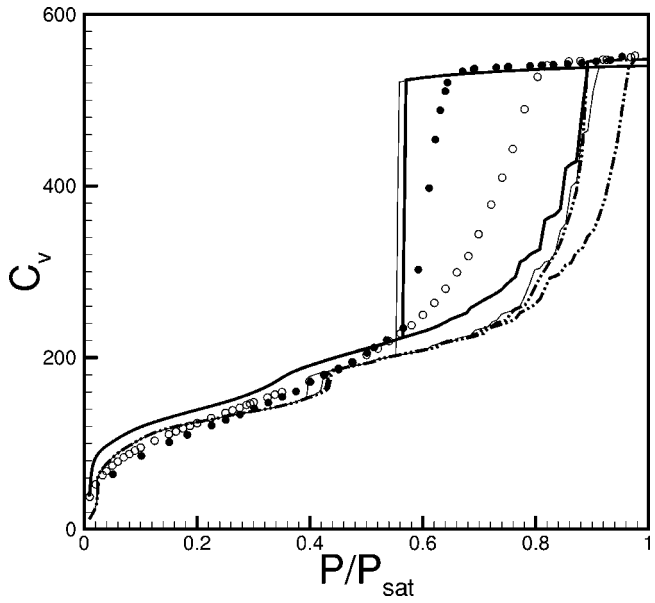


FIG. 11. Adsorption in the center slice $C_v$ (see Fig. 3 caption) versus saturation $P/P_{sat}$ for experimental distributions of triangular pores (thick dotted-dashed line), short-ranged fluid in triangular ink-bottle pores (thin solid line), and longer ranged fluid in triangular ink-bottle pores (thick solid line). Experimental adsorption (open circles) and desorption (filled circles) results are shown [3].

opening would have an enormous impact on the adsorption-desorption isotherms. The pores would now be ink-bottle pores, type I in Fig. 9. Ink-bottle pores may have a much larger hysteresis loop, depending on the neck diameter. The desorption of the simulation pore happens at a similar saturation to the experiment for square pores if a constriction diameter of $10-12\sigma$ is used. The adsorption curves of ink-bottle pores are also shifted to lower saturations than the corresponding straight pores (see Figs. 10 and 11). The use of ink-bottle pores would improve the agreement with the experimental results in creating the correct size of the hysteresis loop and shape of the desorption branch and bring the adsorption branch into slightly better agreement. Another point of note is that the experimental group reported that the adsorption-desorption curves of pores with two pore openings and only one pore opening, types II and III of Fig. 9, were nearly identical [2]. If their system is truly straight pores, this result is very difficult to interpret because the adsorption curves of types II and III simulation pores do not fill or empty at the same saturation. However, if the pores contain constrictions as described, this result makes perfect sense since the small constrictions control the emptying of the pores whether one end is closed off or not. If a type I pore of Fig. 9 had the bottom blocked off, then the small constriction at the top would control the emptying. In Part I, we have already shown that the adsorption behavior of types I and III pores is identical.

*Wall potential*. The strength of the wall potential was chosen to allow the adsorption at low saturations to agree with the experimental results. From Henry's law, it follows that the strength of the wall potential does not have any influence on the pore condensation after the the wall is strong enough to cause complete wetting. In Fig. 12 we have varied the wall strength (keeping it strong enough to always cause complete wetting) and plotted the adsorption versus the saturation for a few cases. The pore condensation is not affected at all while the adsorption behavior at lower saturations is strongly affected by the wall strength for large pore sizes. For smaller pore sizes, the condensation shows some dependence on the wall strength. However, the overall pore filling observed for the distributions is controlled by the larger pore sizes so this

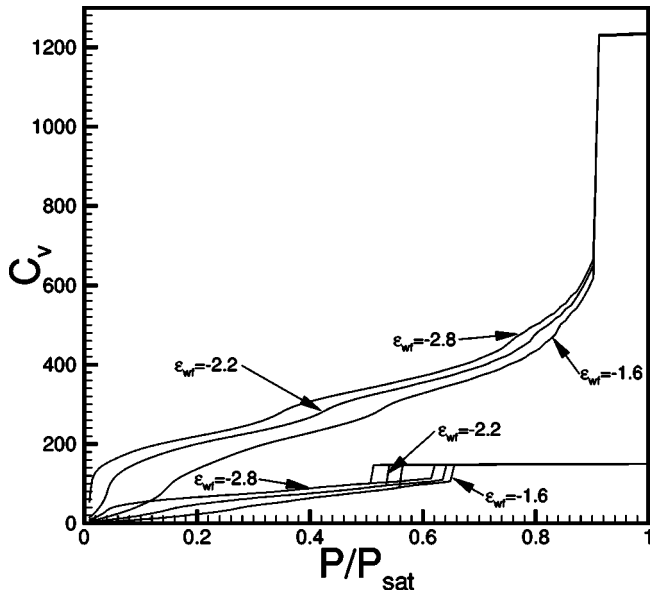


FIG. 12. Adsorption in the center slice $C_v$ (see Fig. 3 caption) versus saturation $P/P_{sat}$ for two triangular ink-bottle pores at three wall strengths.

dependence of the smaller pore sizes does not have a significant impact.

*Fluid-fluid interactions*. A final consideration for the pore results is the details of the fluid-fluid interaction. This study used an interaction limited to the nearest neighbor which we believe captures the significant features of the fluid-fluid interaction. This can be checked by comparing results for this model with one where the interaction range is increased in a realistic manner. For the triangular ink-bottle pores, results with interactions out to the third nearest neighbor were computed. A mapping of the general behavior of the Lennard-Jones potential was used with the minimum of the potential set at the nearest neighbor distance $\sigma$. This potential model has more interacting sites and hence a different critical temperature, $kT_c = 2.53392$, compared to the nearest neighbor model ($kT_c = 1.5$). To properly compare between the two models the same ratio of $T/T_c$ is used. In Fig. 11 the adsorption $C_v$ versus the saturation for an ink-bottle triangular pore is shown plotted for the two different models. The significant differences are that the layering transitions showing hysteresis for the nearest neighbor only model become completely reversible for the model with interactions out to the third nearest neighbor. The other feature is that the pore condensation is shifted to slightly lower saturations than is seen for the nearest neighbor only model. The use of a more detailed potential will improve the agreement in shape of the adsorption at saturations before pore condensation. Surprisingly, the use of such a model also has a minor effect on the location of the pore condensation. The result of the ink-bottle triangular pores with or without interactions out to greater distances has improved the qualitative agreement with the experimental results greatly over that seen for straight pores.

In Fig. 13 a Gaussian distribution centered at 9.25 nm of the triangular ink-bottle pores is shown. This result has an adsorption branch which fills at roughly the same point as the experimental results. The behavior of the curve at lower saturations is not as good as it is for the larger distribution but this could be adjusted by varying the wall-fluid interaction strength. This result has the distribution centered closer to the real result than the value reported for a distribution of cylinders [3].

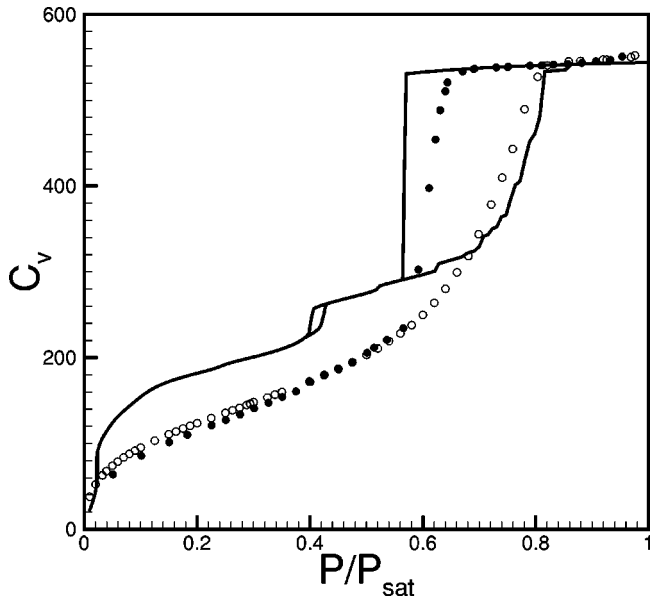


FIG. 13. Adsorption in the center slice $C_v$ (see Fig. 3 caption) versus saturation $P/P_{sat}$ for a Gaussian distribution of triangular pores centered at 9.25 nm. Experimental adsorption (open circles) and desorption (filled circles) results are shown [3].

## IV. CONCLUSIONS

In this paper we have presented calculations describing the adsorption isotherms of distributions of pores with various shapes. It has been shown that for Gaussian distributions the behavior of the various pore shapes is largely similar. The adsorption and desorption branches generally have similar slopes. The location of the filling and emptying has a minor dependence on the pore shape. The largest deviations come about with the introduction of acute angled corners in the pores which influence the slopes of the adsorption and desorption branches compared to the other pore shapes. The results for the Gaussian distributions agree with previous simulation work. However, for pore size distributions centered at larger sizes or with large standard deviations, a departure is seen from this behavior as the pore exterior surface begins to affect the pore desorption. Adsorption isotherms were then calculated for a pore distribution obtained from accurate experimental data. Distributions calculated for straight pores, as implied by the experiment results, did not capture all of the features seen in the experimental work. Consideration of nonideal pore shapes does account for the overall shape of the adsorption curve although the value of the saturation at pore condensation does not agree. The desorption branch and size of the hysteresis loop cannot be reproduced using the simulation model for straight pores. Many possible means of altering the simulation results were considered. Most of these were eliminated as having no effect on the simulation results or not being applicable. Extending the range of the fluid-fluid interaction improved the shape of the adsorption curve at low saturations and shifted the pore condensation by a very small amount. The one alternative considered which had a large effect was introducing constrictions in the system which occupy a small fraction of the total pore length; such constrictions do not contradict any of the experimental data. The simulation results of the ink-bottle pores agree much better with the experimental results. The strange behavior of the experimental data for pores with one end or both ends open is also accounted for if it is assumed that such constrictions are present. Further checks of the experimental system are required to eliminate the possibility that such defect constrictions account for the behavior before other possibilities are considered. The ability of this model to quickly calculate the adsorption isotherms for collections of pores will be useful in future studies of explicit networks of pores.

[1] A. P. Malanoski and F. van Swol, preceding paper, Phys. Rev. E **66**, 041602 (2002).
[2] B. Coasne, A. Grosman, C. Ortega, and M. Simon, *MRS Symposium Proceedings, Dynamics in Small Systems V*, edited by J. M. Drake, J. Klafter, P. Levitz, R. M. Overney, and M. Urbakh (Materials Research Society, Warrendale, PA, 2001).
[3] B. Coasne, A. Grosman, N. Dupont-Pavlovsky, C. Ortega, and M. Simon, Phys. Chem. Chem. Phys. **3**, 1196 (2001).
[4] B. Coasne, A. Grosman, C. Ortega, and M. Simon, Phys. Rev. Lett. **88**, 256102 (2002).